

# Synthesis of yttria nanopowders for transparent yttria ceramics

Lei Wen<sup>a,b,\*</sup>, Xudong Sun<sup>b</sup>, Qi Lu<sup>a</sup>, Guoxiang Xu<sup>a</sup>, Xiaozhi Hu<sup>c</sup>

<sup>a</sup> Department of Applied Chemistry, College of Chemistry and Molecular Engineering, Peking University, Beijing 100871, China

<sup>b</sup> School of Materials and Metallurgy, Northeastern University, Shenyang 110004, China

<sup>c</sup> Department of Mechanical Engineering, University of Western Australia, Australia

Received 6 December 2004; accepted 2 September 2005

Available online 25 October 2005

## Abstract

This paper describes a precipitation process for synthesizing nanocrystalline yttria powder and sintering transparent yttria ceramics. Hydroxide precursor of  $Y_2O_3$  with an approximate composition of  $Y_2(OH)_5NO_3 \cdot H_2O$  was synthesized by using ammonia water as precipitant and yttrium nitrate as the starting salt. Employing appropriate striking method and optimum synthetic conditions, yttrium hydroxide with a card-house or spherical structure can be formed. It was found that normal striking derived powders have higher sinterability than reverse striking derived powders. The addition of a small amount of ammonia sulfate in the yttrium nitrate solution reduces the agglomeration and particle size of the produced yttria powders. Nanocrystalline yttria powders (60 nm in average size) was obtained by calcining the precursor at 1100 °C for 4 h. Transparent yttria ceramics were fabricated from the nano  $Y_2O_3$  powders by vacuum sintering at 1700 °C for 4 h. In the wavelength of 1000 nm, the in-line transmittance reaches 52%.

© 2005 Elsevier B.V. All rights reserved.

**Keywords:** Powders-chemical preparation; Sintering; Transparency;  $Y_2O_3$

## 1. Introduction

Yttria finds potential application because of its high corrosion resistivity, thermal stability and transparency over a wide wavelength region, i.e., from violet to infrared light [1]. Moreover, yttria material can also act as a laser host material [2,3]. This material is mainly manufactured by using powder technology, i.e., sintering. The typical sintering temperature for producing transparent  $Y_2O_3$  are about 2000 °C under normal pressure for long periods [4,5] or at about 1500 °C under high pressure [6,7], and some sintering aids were used to enhance the densification, such as  $ThO_2$  [2,5],  $La_2O_3$  [8],  $HfO_2$  [3], and  $LiF$  [7]. In recent years, some fabrication methods have been successfully used to produce well-sinterable yttria powders. Saito et al. reported a carbonate precipitation method for synthesizing highly sinterable yttria powder [1]. By controlling the precipitate

temperature and doping with sulfate ions, Ikegami et al. synthesized thin flakes of yttrium hydroxide that have a card-house structure. Well-sinterable  $Y_2O_3$  nanopowders of high-purity have been obtained by calcining the hydroxide precursor at 1100 °C for 4 h and the sintered body showed transparency [9].

In this paper, we have used ammonia water as the precipitant to synthesize yttrium hydroxide precursor. The effect of the precipitation process on morphology, size, and sinterability of the precursor and resultant yttria powders are investigated. The sintering and optical properties of the transparent yttria ceramics have also been studied.

## 2. Experimental

Yttria powder (99.99%, Changchun, China) was dissolved in high-purity nitric acid, and then was diluted with deionized water to the concentration of 0.26 M. To investigate the effect of ammonia sulfate for some specimens, 0.9 g ammonia sulfate was added to a 500 ml yttrium nitrate solution. Ammonia water (2 M, reagent grade) was used

\* Corresponding author.

E-mail addresses: [wenlei@pku.edu.cn](mailto:wenlei@pku.edu.cn), [wenleicn1974@163.com](mailto:wenleicn1974@163.com) (L. Wen).

as the precipitant. During precipitation process, reverse striking means the addition of the solution containing the precursor metal ions to the precipitating agent, and the opposite is called normal striking. In the present work, both striking methods were used and the slow addition rate of 5 ml/min was chosen. Then, the precipitate slurry was aged for 3 h with mild agitation by a magnetic stirrer. The precipitate slurry was filtrated and washed with deionized water for four times to remove the  $\text{NH}_4\text{NO}_3$  by-product. After washing, the precipitate slurry was dried at 60 °C for 24 h. The dried cake was crushed in an alumina mortar and pestle, and subsequently was calcined at selected temperatures under flowing oxygen to obtain yttria powder.

For sintering, powders were first dry pressed manually ( $\sim 20$  MPa pressure) into small cylinders with a diameter of 13 mm and a thickness of 3 mm in a steel die and then isostatically compacted at a pressure of 200 MPa. The pellets were sintered at 1700 °C for 4 h under vacuum of  $1.3 \times 10^{-3}$  Pa in a furnace with molybdenum heating element (VSF-7, Shenyang, China). Phase identification was performed via X-ray diffractometry (XRD) (Model D/MAX-RB, Japan), using nickel-filtered  $\text{Cu K}\alpha$  radiation and a scanning speed of  $2\theta = 8^\circ/\text{min}$ . A transmission electron microscope (TEM, Philips EM420) was used to observe the morphologies of the precipitate precursor and the  $\text{Y}_2\text{O}_3$  powders. Relative density of the sintered specimens was measured by the Archimedes method, which used water as the immersion medium. The sintered specimens were thermally etched at 1500 °C for 2 h in air. Microstructures of the polished surface of the specimens were observed using scanning electron microscopy (SEM, EPM-810Q). Specimens for transmittance measurement were cut into 1.5-mm-thick slices and both surfaces were mirror-polished. Transmittance of the transparent yttria ceramics was measured over the wavelength region from 200 to 1200 nm using a spectrometer (DMR-22, Germany).

### 3. Results and discussion

#### 3.1. Morphology of the precursor

For different striking methods, pH variation of the reaction system is obvious. The relation between pH and ammonia water or  $\text{Y}(\text{NO}_3)_3$  solution added as reactant is shown in Fig. 1. If the  $\text{Y}(\text{NO}_3)_3$  solution is added to the AW (ammonia water) solution (reverse striking), because the original concentration of the AW solution is much higher than that of the  $\text{Y}(\text{NO}_3)_3$  solution, in such a mixed method,  $\text{Y}^{3+}$  reacts immediately with  $\text{OH}^-$  to produce precipitate precursor and the pH value of the system drops gradually. For normal striking method, the initial pH value of the mother salt solution is about 5.0. The plateau, which begins at a pH of about 6.7, indicates that the precipitate is formed and the  $\text{OH}^-$  depleted. When the pH is above about 8.0, the precipitation is completed, and the rapid increase in the pH of the curve is a result of simply adding excess ammonia water to the system.

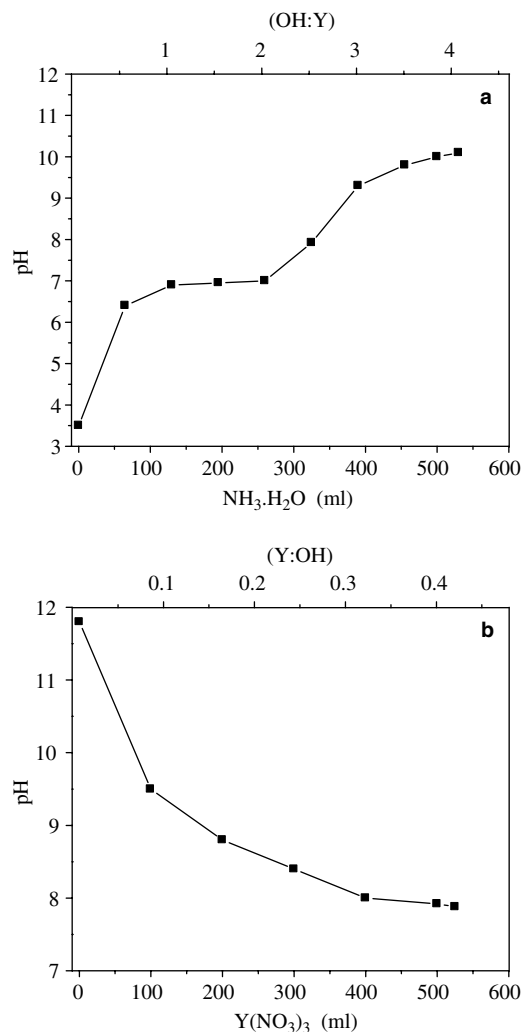


Fig. 1. Relationship between pH and amount of  $\text{NH}_3 \cdot \text{H}_2\text{O}$  or  $\text{Y}(\text{NO}_3)_3$  during different striking methods: (a) normal striking and (b) reverse striking method.

The morphology of precursor formed during precipitation is strongly influenced by the precipitation conditions, such as the final pH value and striking methods. TEM observation indicates that the precursor precipitate has a platelet-like structure in a manner similar to a house of cards (Fig. 2(a)) at low pH value during normal striking method. When the precipitates are formed at a higher pH, as shown in Fig. 2(b), it becomes more equiaxed, and the card-house structure of the precursor are more likely to collapsed. The morphology of the yttrium hydroxide precursor and variation of pH value during striking process were consistent with the work of Voigt [10].

Fig. 3 is the morphology of the precipitate obtained by reverse striking method at different pH values. It can be seen that the aggregates became dense, and the card-house structure disappeared.

According to Voigt [10], variation of precipitate morphology can attribute to the difference of supersaturation

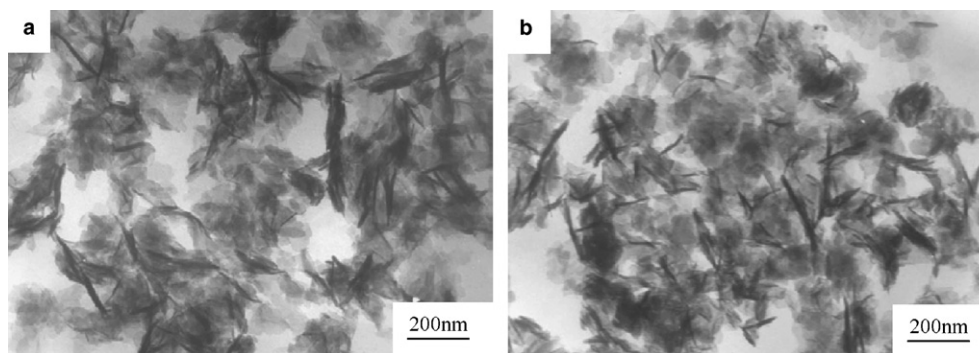


Fig. 2. TEM morphology of the precursor produced by the normal striking method: (a) pH = 7.92 and (b) pH = 10.0.

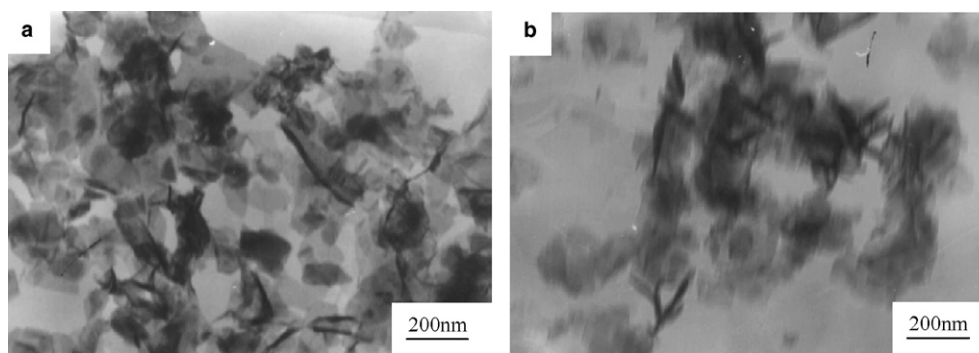


Fig. 3. TEM morphology of the precursor produced by the reverse striking method: (a) pH = 7.92 and (b) pH = 10.0.

levels during different striking conditions. In precipitation, very high levels of supersaturation are created and homogeneous nucleation predominates. Derived from classical nucleation theory, the rate of homogeneous nucleation can be expressed as

$$B = K \cdot e^{-\left(\frac{16\pi\sigma^3 M^2}{3(kT)^3 \rho^2 N^0 \ln^2(S)}\right)},$$

where  $\sigma$  is the interfacial energy between crystal surface and liquid,  $M$  is the molecular weight of the solid,  $\rho$  is the density of the solid,  $N^0$  is Avogadro's number,  $S$  is supersaturation ratio,  $k$  is Boltzmann's constant,  $T$  is the absolute temperature, and  $K$  is a function of temperature and supersaturation. It can be seen that the nucleation rate increases as the supersaturation increases. The supersaturation ratio,  $S$ , is the ratio of the solute concentration,  $c$ , in the solution to the total solute concentration,  $c_s$ , at equilibrium. James Alan Voigt calculated estimated values of the supersaturation,  $S = c/c_s$ , as shown in Fig. 4.

For reverse striking method or high pH conditions of normal striking, supersaturation levels are much higher than that of low pH condition or normal striking.

Yttrium hydroxynitrate tend to assume a platelet-like morphology. Prior to us, the work on hydrothermally prepared trivalent lanthanide (including yttrium) hydroxynitrates via precipitation method was conducted by Voigt [10] and Haschke and coworkers [11,12]. According to their work, such phenomena can be inferred from the crystal structure of yttrium hydroxynitrates. Perfect

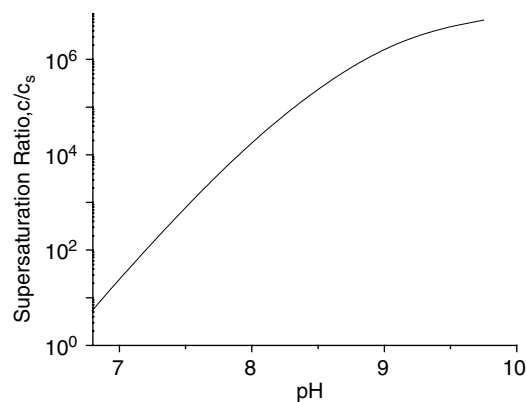


Fig. 4. Relationship between supersaturation ratio and pH value.

yttrium hydroxynitrates are layered structures composed of alternating layers of hydroxide-coordinated metal ions and ions. The rapidly growing faces are perpendicular to the planes of the layers. Growth by addition of new layers is slower than growth at the edges of the layers. So this hydroxide precursor is mainly up of irregularly shaped particles, and tends to form a platelet-like morphology. But when supersaturation levels increased, more rapid crystal growth will occur. This rapid crystal growth tends to decrease the preferential growth of the crystallites. Thus, higher supersaturation conditions generally form more equiaxed crystallites and platelet morphology of the precursor disappeared [10].

### 3.2. Morphology of the products

Fig. 5 shows TEM morphologies of the  $Y_2O_3$  powders obtained by calcining four typical kinds of precipitates at 1100 °C for 2 h. A common feature of the precipitation derived powders is that they all have some agglomerates. However, different synthetic conditions caused some differences in the dispersivity of these powders. Compared with powder a (Fig. 5(a)), powder b–d, were more severely agglomerated. Although powder a still has some agglomeration, the powder shows the highest dispersivity of all these powders. It is mainly composed of round shaped particles rather than irregularly large particles with sharp edges, like b–d.

### 3.3. Composition of the precursor

The present work showed that both the appropriate striking method and low final pH value at the end of the precipitation process are essential to the fabrication of highly sinterable yttria powders and transparent ceramics, as was shown below. So, the composition of this kind of precipitate precursor was determined by XRD, the final pH value of the precipitation process of normal striking is about 7.92. If ammonia water is added to a rare earth salt solution, the rare earth hydroxide precipitates, and the ratio of  $OH^-/Re^{3+}$  changes from 2.5 to 3.0 depending on the cation. Thus, the composition of the precursor will be  $Y_2(OH)_5(NO_3) \cdot H_2O$  and this is proved by the XRD analyses (Fig. 6). After calcining at temperatures  $\geq 700$  °C for 2 h, the precursor transforms to the yttria phase (Fig. 6).

### 3.4. Effect of $SO_4^{2-}$ on the morphology of $Y_2O_3$ powders

According to Ikegami et al. [9,13], nanocrystalline  $Y_2O_3$  powders can be synthesized by calcining  $SO_4^{2-}$  doped yttrium hydroxide precursor. Ikegami et al. also demonstrated that both the aging of yttrium hydroxide at temperatures lower than room temperature and doping with sulfate ions are essential to the fabrication of highly sinterable yttria powders [9,13].

In this paper, we found that both striking methods and pH value at the end of the precipitation process has a significant effect on the sinterability of the resultant yttria powders. So, for the fabrication of transparent yttria ceramics, optimum synthetic conditions of striking methods was used, and at the same time, lower temperature aging of hydroxide and  $SO_4^{2-}$  doped techniques were also employed.

Fig. 7 shows the morphology of yttria powders obtained by  $SO_4^{2-}$  doped  $Y_2(OH)_5(NO_3) \cdot H_2O$ . The precursor was calcined at 1100 °C for 4 h. It can be seen that the sulfate doped yttria powder is well dispersed and has a smaller particle diameter (about 60 nm).

$Y_2(OH)_5(NO_3) \cdot H_2O$  has a positive  $\zeta$  potential in aqueous solution [10], hence  $SO_4^{2-}$  can adsorb onto the surface of  $Y_2(OH)_5(NO_3) \cdot H_2O$  particles due to the electrostatic force. The  $SO_4^{2-}$  has a higher decomposition temperature than hydroxides and its existence at comparatively high temperature may reduce the element diffusion between particles, resulting in a smaller particle size. Its decomposition at high temperatures is also beneficial for the dispersion of powder [14].

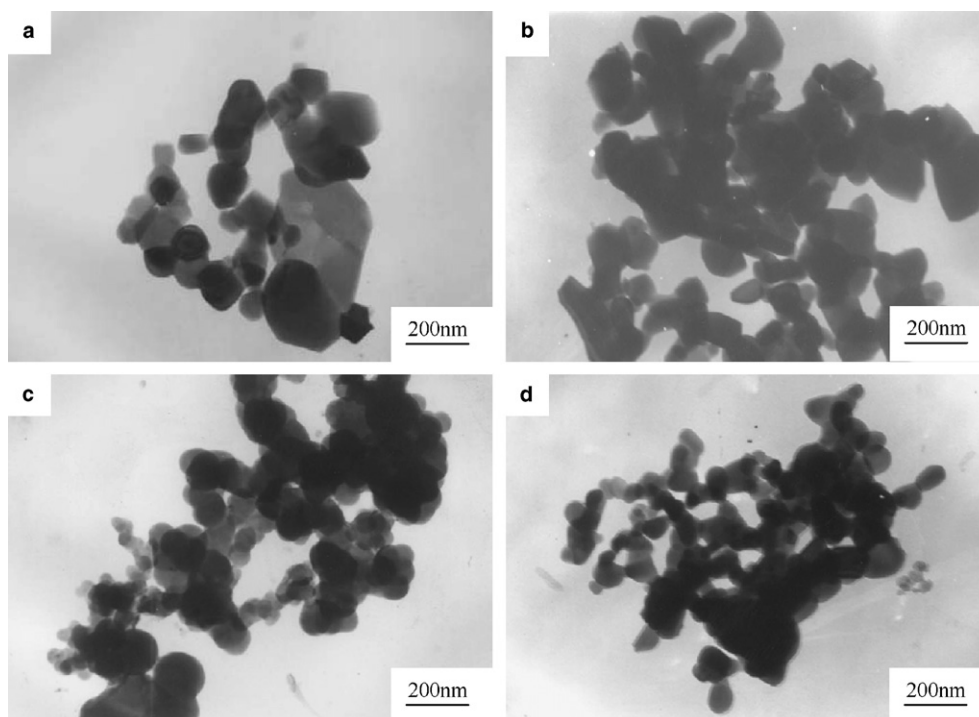


Fig. 5. TEM morphology of the  $Y_2O_3$  powders: (a) normal striking method, pH = 7.92; (b) normal striking method, pH = 10; (c) reverse striking method, pH = 7.92 and (d) reverse striking method, pH = 10.

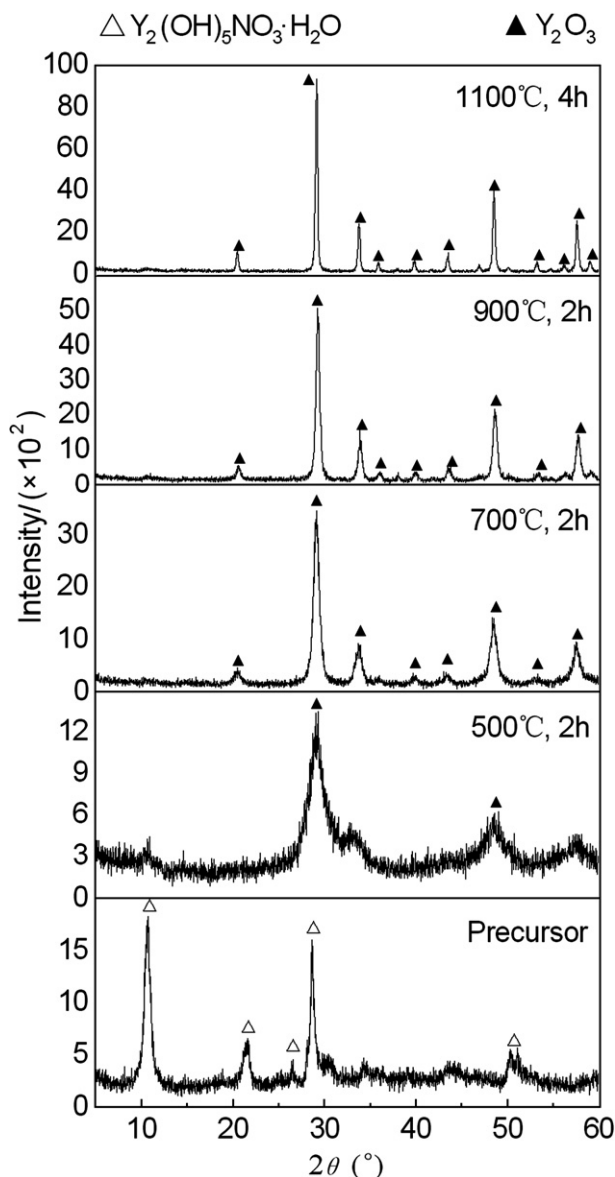


Fig. 6. XRD spectra of the precursor and the calcined powders.

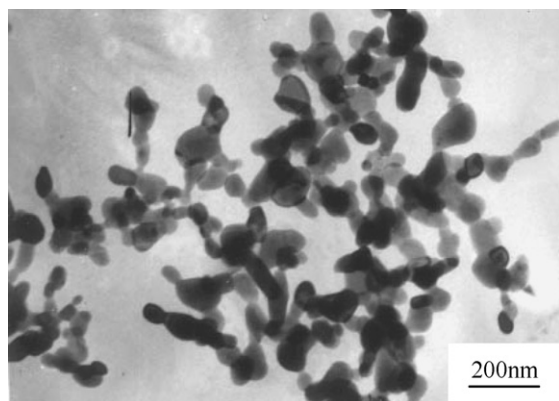


Fig. 7. TEM morphology of the  $Y_2O_3$  powder made by doping with sulfate ions.

### 3.5. Sintering of the $Y_2O_3$ powder

Powders for sintering were synthesized via the normal and reverse striking method. To compare sinterability of the yttria powders obtained by different striking methods, all the hydroxide precursor was calcined at 1100 °C for 1 h under flowing oxygen to yield yttria powders. Fig. 8 illustrates the relationship between the relative density of the sintered samples and pH value.

It can be seen that normal striking derived powders exhibit higher sinterability than reverse striking derived powders. For the normal striking method, low-pH derived powders show the highest sinterability, the relative density is about 96.2%. Large particle sizes and severe agglomeration are responsible for lower sintering reactivity of the other yttria powders. The yttria powder synthesized from the normal striking method at low pH value has the least tendency of agglomeration and somewhat smaller particle size, resulting in the highest density of the sintered body. Although the powder from this method reached almost theoretical density, for fabrication of transparent ceramics with theoretical density is not enough. In the present work, it was found that  $SO_4^{2-}$  doped  $Y_2(OH)_5(NO_3) \cdot H_2O$  derived powders can be densified to nearly full density by vacuum sintering at 1700 °C for 4 h and the sintered body showed transparency. Fig. 9 shows the sintered yttria ceramics, of which the precursor were normal striking derived  $Y_2(OH)_5(NO_3) \cdot H_2O$ ,  $SO_4^{2-}$  doped  $Y_2(OH)_5(NO_3) \cdot H_2O$ , aging at 50 °C, and  $SO_4^{2-}$  doped  $Y_2(OH)_5(NO_3) \cdot H_2O$ , aging at 0 °C, respectively. Each pellet is

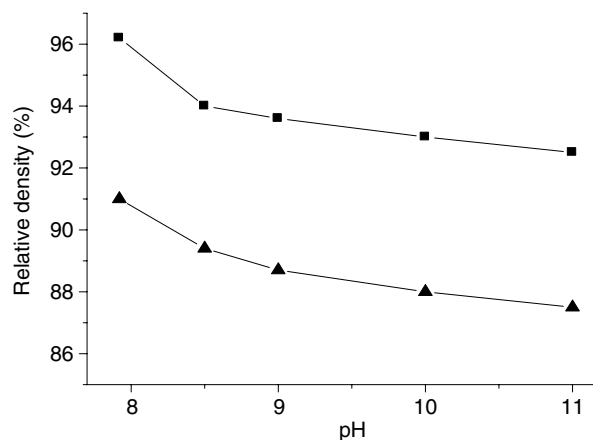


Fig. 8. Relationship between relative density and final pH (a) normal striking and (b) reverse striking method.



Fig. 9. Photograph of  $Y_2O_3$  ceramics (a) striking at 0 °C (b) striking at 50 °C and (c)  $SO_4^{2-}$  undoped.

~10.5 mm in diameter and ~1.5 mm thick. It can be seen that low aging temperature and  $\text{SO}_4^{2-}$  doped can lead the powders sintered to transparency, whereas those precursor precipitated at higher temperature is opaque. The present results were consistent with the work of Ikegami et al. [9]. Conventional techniques using for synthesizing transparent or translucent yttria ceramics need high temperature or some sintering aids to prevent grain-boundary break-away. In the present work, the green compact is homogeneous, since the  $\text{SO}_4^{2-}$  doped precursor derived powder is well dispersed and exhibit a narrow particle size distribution, and hence abnormal grain growth did not occur. Pores which remain at grain boundaries can be eliminated easily, and thus the sintering temperature is about 300 °C lower than conventional pressureless sintering techniques.

Fig. 10 shows the microstructure of the polished and etched yttria specimen sintered at 1700 °C. The sintered body has a homogeneous microstructure with an average grain size about 20  $\mu\text{m}$ .

Light transmittance is a main parameter in elevating the optical properties of the transparent ceramics. Fig. 11

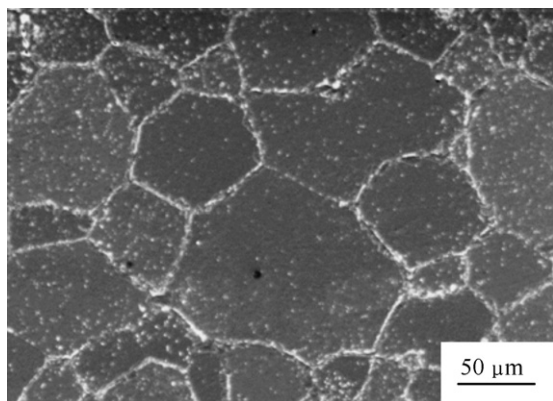


Fig. 10. SEM photograph showing the microstructure of polished surface of the specimen sintered at 1700 °C (small white dots are due to alumina from the abrasive paper used for polishing media).

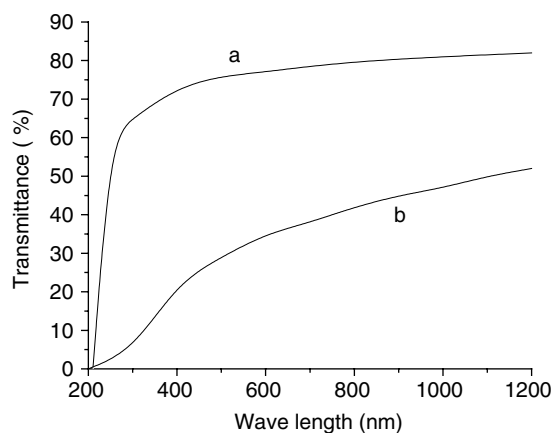


Fig. 11. Optical transmission spectra of a  $\text{Y}_2\text{O}_3$  single crystal and transparent  $\text{Y}_2\text{O}_3$  ceramics (a) single crystal [1] and (b) transparent yttria ceramics.

shows the in-line transmittance spectra in the wavelength region from 200 to 1200 nm for the specimens sintered at 1700 °C for 5 h. The data of a single-crystal are also shown.

In the measured wavelength region, the highest optical transmittance is about 52%. The in-line transmittance increases with increasing wavelength. This can be attributed to the difference between a single crystal and polycrystalline ceramics. There are some scattering centers in the ceramics. When the optical scattering center is significantly smaller than the wavelengths, the scattering intensity can be determined by Rayleigh's equation, i.e., the scattering intensity increases proportionally with  $\lambda^{-4}$ , where  $\lambda$  is the wavelength. Thus, the scattering intensity increases with decreasing wavelength [15].

#### 4. Conclusions

1. Hydroxide precipitation, employing  $\text{Y}(\text{NO}_3)_3$  as the starting salts and ammonia water as the precipitant, have been used to synthesize yttria powders. Chemical precipitation process was optimized. It was found that both striking methods and pH value at the end of precipitation process influences the morphology of yttrium hydroxide precursor, which in turn significantly affects sinterability of the resultant yttria powders.
2. For normal striking method, the hydroxide precursor produced at low final pH value has a platelet-like structure in a manner similar to a house of cards. When the precipitates are synthesized at high pH conditions or by reverse striking method, platelet-like morphology of the precursor tend to disappear.
3. Normal striking derived powders have higher sinterability than reverse striking derived powders. For normal striking method, low pH derived powders show the highest sinterability, while the maximum relative density reaches 96.2%.
4. The addition of a small amount of ammonia sulfate to the yttrium nitrate solution can yield highly reactive yttria powders. The resultant yttria powders is fine (60 nm in average primary particle size), narrow in size distribution and loosely agglomerated.
5. Using such  $\text{Y}_2\text{O}_3$  powders, after vacuum sintering at 1700 °C for 4 h, transparent yttria ceramics have been fabricated. In the wavelength of 1000 nm, the in-line transmittance reaches 52%.

#### Acknowledgements

Supported by the Trans-Century Training Program Foundation for the Talents by the Ministry of Education of China, the Natural Science Foundation of China (Grant No. 50172010) and the Natural Science Foundation of Liaoning Province (Grant Nos. 2001101002 and 9910300102).

**References**

- [1] N. Saito, S. Matsuda, T. Ikegami, *J. Am. Ceram. Soc.* 81 (1998) 2023.
- [2] C. Greskovich, J.P. Chernoch, *J. Appl. Phys.* 44 (1973) 4599.
- [3] A. Ikesue, K. Kamata, *J. Am. Ceram. Soc.* 79 (1996) 359.
- [4] Y. Tsukuda, A. Muta, *J. Ceram. Soc. Jpn.* 84 (1976) 585.
- [5] C. Greskovich, K.N. Woods, *Am. Ceram. Soc. Bull.* 52 (1973) 473.
- [6] S.K. Dutta, G.E. Gazza, *Mater. Res. Bull.* 4 (1969) 791.
- [7] K. Majima, N. Niimi, M. Watanabe, *J. Jpn. Inst. Met.* 57 (1993) 1221.
- [8] W.H. Rhodes, *J. Am. Ceram. Soc.* 64 (1981) 13.
- [9] T. Ikegami, T. Mori, Y. Yajima, *J. Ceram. Soc. Jpn.* 107 (1999) 297.
- [10] J.A. Voigt, Ph.D. dissertation, Iowa State University, 1986.
- [11] J.M. Haschke, *Inorg. Chem.* 13 (1974) 1812.
- [12] J.M. Haschke, L. Eyring, *Inorg. Chem.* 10 (1971) 2267.
- [13] T. Ikegami, J.G. Li, T. Mori, et al., *J. Am. Ceram. Soc.* 85 (2002) 1725.
- [14] L. Wen, X.D. Sun, Z.M. Xiu, et al., *J. Euro. Ceram. Soc.* 24 (2004) 2681.
- [15] A. Ikesue, K. Yoshida, T. Yamamoto, *J. Am. Ceram. Soc.* 80 (1997) 1517.